Journal Pre-proof

Flow patterns in shallow rectangular reservoirs with open channel inlet or pipe flow inlet at various depths: An experimental study

El Mehdi Chagdali, Kamal El Kadi Abderrezzak, Sébastien Erpicum, Cédric Goeury, Matthieu Secher, Benjamin Dewals

PII: S1001-6279(25)00004-6

DOI: https://doi.org/10.1016/j.ijsrc.2025.01.004

Reference: IJSRC 616

To appear in: *International Journal of Sediment Research*

Received Date: 23 August 2023

Revised Date: 4 January 2025

Accepted Date: 16 January 2025

Please cite this article as: Chagdali E.M., El Kadi Abderrezzak K., Erpicum S., Goeury C., Secher M. & Dewals B., Flow patterns in shallow rectangular reservoirs with open channel inlet or pipe flow inlet at various depths: An experimental study, *International Journal of Sediment Research*, https://doi.org/10.1016/j.ijsrc.2025.01.004.

Flow patterns in shallow rectangular reservoirs with open channel inlet or pipe flow inlet at various depths: An experimental study

El Mehdi Chagdali[a,b,c,*], Kamal El Kadi Abderrezzak[a,b], Sébastien Erpicum[c], Cédric Goeury[a,b], Matthieu Secher[d], Benjamin Dewals[c]

[a] *National Laboratory for Hydraulics and Environment (LNHE), EDF R&D, Chatou 78400, France*

[b] *Saint Venant Laboratory for Hydraulics, University Paris-Est, Chatou 78400, France*

[c] *Research Group of Hydraulics in Environmental and Civil Engineering (HECE), University of Liège, Liège 4000, Belgium*

[d] *Hydraulics Engineering Center (CIH), EDF Hydro, La Motte-Servolex 73290, France*

- Corresponding author. E-mail: chagdalielmehdi@gmail.com (E. M. Chagdali)

Flow patterns in shallow rectangular reservoirs with open channel inlet or pipe flow inlet at various depths: An experimental study

Abstract

This study experimentally assesses the influence of varying the inlet boundary condition on the flow patterns in rectangular shallow reservoirs. Two types of inlet boundary conditions were compared: a free surface inlet channel, and a pressurized circular inlet jet positioned at three different elevations over the flow depth (centroid of the inlet jet situated at 25%, 50%, or 75% of the flow depth). The outlet boundary condition was a free surface channel in all cases. Twenty-two experiments were done with two distinct reservoir lengths (length-to-width ratios of 1.1 and 2.0) and three hydraulic boundary conditions (Froude numbers of 0.14, 0.16, and 0.21). Velocity fields were measured with Large-Scale Particle Image Velocimetry (LSPIV) at the surface, and with an Acoustic Doppler Velocity Profiler (ADVP) at several cross sections. The flow patterns are greatly influenced by the inlet boundary condition and the reservoir geometry, but to a lesser extent by the hydraulic boundary condition. For an inlet circular jet located near the reservoir bottom, an unstable flow type, changing over time in a chaotic manner, was observed regardless of the reservoir length and of the inlet flow rate. The same type of unstable flow pattern was observed for a relatively long reservoir and the lowest tested flow rate, irrespective of the vertical positioning of the inlet jet. In all other tested configurations, a steady reattached jet was found in the reservoir equipped with a pressurized inlet jet. In addition to providing new knowledge on flow patterns in shallow reservoirs with an inlet jet, the experimental data presented here will prove valuable for evaluating flow computational models.

Keywords: Shallow reservoirs; Pressurized jet; Laboratory experiments; Large-scale particle image velocimetry (LSPIV); Acoustic Doppler velocity profiler (ADVP)

1. Introduction

Shallow reservoirs are hydraulic structures widely used in civil and environmental engineering (e.g., stormwater basins, sediment and pollutant trapping tanks, water storage basins in pumped-storage hydropower plants, aquafarming tanks). Loss of effective storage capacity due to sedimentation reduces the services these reservoirs can deliver (Schleiss et al., 2016). Predicting the flow field in shallow reservoirs is a prerequisite for reliably predicting sedimentation patterns, and, thus, for optimizing reservoir design, management, and maintenance. Flow patterns and sedimentation rate in a shallow reservoir depend on its geometrical shape, hydraulic boundary conditions (e.g., type and position of inlet and outlet), and sediment characteristics (Camnasio et al., 2013; Dufresne et al., 2010; Kantoush, 2008). Previous laboratory experiments have revealed complex flow patterns (e.g., two-dimensional horizontal large-scale turbulent structures, eddies, and recirculation zones, three dimensional flow structures), even for simple geometric configurations, such as rectangular shallow reservoirs (Dewals et al., 2008; Dufresne et al., 2010; Kantoush, 2008; Shoarinezhad et al., 2023). The current study focuses on rectangular shallow reservoirs with either a free surface inlet channel or a pressurized circular inlet jet.

Flow entering shallow reservoirs can be regarded as a flow passing through a narrow inlet channel entering a suddenly expanded channel.

As reviewed by Casarsa and Giannattasio (2008), Moallemi and Brinkerhoff (2016), and Shoarinezhad et al. (2023), laboratory studies have been done for laminar flow in symmetric sudden expanded channels. For low inlet Reynolds numbers, the observed flow patterns are symmetric with respect to the reservoir centerline, while they become asymmetric (i.e., with a reattachment point on either of the channel sidewalls) above a critical value of the inlet Reynolds number (Durst et al., 1993). Limited experimental studies have been done on turbulent free surface flows in symmetric sudden double-lateral expansions (Escudier et al., 2002). For inlet Reynolds numbers ranging from 4×10^4 to 10^5, Abbott and Kline (1962) observed asymmetric flow patterns for large expansion ratios. Such findings were confirmed by Casarsa and Giannattasio (2008), Mehta (1981), and Restivo and Whitelaw (1978) among others.

Kantoush (2008) investigated the flow pattern in rectangular shallow reservoirs with free surface channels at the inlet and outlet. The reservoir width and length were systematically varied. The Froude number Fr (defined as $U_{in}/(gH)^{0.5}$, with U_{in} the inlet flow velocity, g the gravity acceleration, and H the flow depth) was varied in the range of 0.05–0.43. Kantoush (2008) and Kantoush et al. (2008a) reported five types of flow patterns: symmetric with two reattachment points (S2), asymmetric with one reattachment points (A1), asymmetric with two reattachment points (A2), symmetric without reattachment point (S0), and a meandering jet. One additional asymmetric flow pattern (A3) was later identified experimentally by Dufresne et al. (2010) who provided a criterion to predict the occurrence of detached (symmetric) or reattached flow using a new shape factor defined as $SF = L_1/(\Delta B^{0.6} b^{0.4})$, with L the reservoir length, b the inlet channel width, and $\Delta B = (B - b)/2$ the width of the sudden expansion, where B is the reservoir width. For Fr = 0.20, Dufresne et al. (2010) found symmetric detached flows when SF < 6.2 (i.e., relatively short reservoirs) and asymmetric reattached flows for SF > 6.8 (i.e., relatively long reservoirs). Near the transition between symmetric and asymmetric flows, unstable flow patterns were identified. Camnasio et al. (2011, 2013) experimentally examined the effect of varying the position of boundary inlet and outlet open channels and classified the flow field in shallow rectangular reservoirs into a channel-like type, two symmetric, and two asymmetric stable types, based on the reservoir expansion and aspect ratios. Building upon the work of Camnasio et al. (2013), Miranda et al. (2018) analyzed the flow pattern in a shallow rectangular reservoir, examining six different inlet and outlet channel positions. They also assessed the impact of three different flow rates on the results, with a Froude number ranging from 0.09 to 0.12. Choufi et al. (2014) examined the effect of reservoir bottom roughness. Peltier et al. (2014) investigated oscillatory flows (i.e., meandering jets) and identified threshold values on the shape factor and Froude number to characterize the occurrence of a meandering jet type flow. Miozzi and Romano (2020) studied meandering jets in a rectangular reservoir with an open channel at the inlet and a weir along the downstream side of the basin.

Limited work has been published on the flow pattern in shallow reservoirs with a circular jet as the inlet boundary condition. Adamsson et al. (2005) observed two large symmetric recirculations in a rectangular basin equipped with an inlet horizontal circular pipe and a weir at the outlet. The basin

geometry and the positioning of the inlet jet were kept constant. Dufresne (2008) did experiments in a rectangular reservoir of fixed geometry, with a circular pipe at the inlet and a weir at the outlet (extending over the whole reservoir width). The experiments were carried out with water and polystyrol particles. He observed an asymmetric steady flow for water depth lower or equal to 0.015 m and a symmetric steady flow for water depth above 0.030 m. A pseudo periodic regime appeared between these two cases. The current study addresses the effect of the inlet boundary condition on flow patterns in rectangular shallow reservoirs based on laboratory experiments: free surface rectangular inlet channel (reference case) and a turbulent circular inlet jet; the outlet boundary condition being a free surface channel for both cases.

The current research includes twenty-two novel laboratory experiments. Unlike Adamsson et al. (2005) and Dufresne (2008), not only the hydraulic boundary conditions but also the reservoir length and the positioning of the inlet pipe were varied in this new set of experimental tests. Thanks to detailed flow velocity measurements, a novel typology of flow patterns is proposed, involving unstable and steady reattached jets. The current experimental results contribute to enhancing the understanding of flow dynamics in rectangular reservoirs. They also provide new insight into the relative influence of the setup geometry and of the hydraulic boundary conditions on the flow fields. Finally, they provide valuable data for evaluating and improving computational flow models.

2. Experimental setup and test program

Twenty-two experimental tests were done in a laboratory setup constructed in the hydraulic laboratory of the University of Liege, Belgium. The setup is based on the same facility as previously used by Dufresne et al. (2010) and Peltier et al. (2014). The rectangular reservoir was inserted in a 10.4 m long horizontal flume (Fig. 1(a)). The reservoir width was kept constant and equal to the flume width: B = 0.985 m, while the length, L_1, was changed by solid blocks (Fig. 1(a)). The flume bottom and walls were fixed and made of glass. In all configurations, the reservoir outlet was a free surface channel of width b_o = 0.08 m. The flow depth, H, at the outlet of the reservoir was set at 0.10 m in all tests (i.e., shallowness ratio H/B = 0.10). Two types of inlet boundary conditions were considered: either a free surface rectangular channel or a circular jet.

For configurations with a free surface inlet channel, the inlet and outlet channels were located along the reservoir centerline, on opposite sides. The width of the inlet channel was set to $b = 0.08$ m (aspect ratio of 0.8), leading at the entrance of the reservoir to a sudden lateral expansion of $\Delta B = 0.4525$ m on both sides. The flow enters the flume from an upstream stilling basin through a porous screen, which aims at preventing fluctuations in water level and favoring the establishment of a fully developed velocity profile. Further downstream, the flow contracts through a converging section to match the width of the inlet channel (Fig. 1(a)). The inlet channel is 2.00 m in length.

In the case of a circular jet at the inlet, the inflow pipe was connected to a PVC tube, of 0.04 m in diameter, fixed perpendicularly to a movable vertical plate (Figs. 1(b) and 1(c)). The vertically movable circular tube allows adjusting the positioning of the inlet jet over the flow depth. Three different positions were tested: close to the reservoir bottom ($Z_{jet}/H = 0.20$), at mid-depth ($Z_{jet}/H = 0.50$), and close to the water surface ($Z_{jet}/H = 0.75$), with Z_{jet} the elevation of the inlet pipe centroid above the reservoir bottom. The inlet tube and outlet channel were aligned with the reservoir centerline. The inlet pipe had a length of 1.0 m, resulting in a length-to-diameter ratio of 25. This length is sufficient to ensure fully developed flow at the reservoir inlet. Indeed, for the three inflow discharges considered in the experiments (0.0005, 0.00175, and 0.0030 m³/s), the Reynolds number (Re) in the pipe was 1.59×10^4, 5.57×10^4, and 9.55×10^4, respectively. For turbulent flow, the recommended entrance length L_e may be estimated as $L_e \approx 1.359\mathrm{Re}^{1/4}D$, where D is the hydraulic diameter of the pipe or channel (Çengel & Cimbala, 2018). This leads to values for L_e of 0.61, 0.84, and 0.96 m, respectively. Hence, the pipe length in the laboratory was long enough to ensure fully developed flow for all considered inflow discharges. Unlike in the case of shallow reservoirs equipped with an open-channel inlet, pressurized flow at the inlet leads to a non-uniform vertical distribution of flow velocity and 3D flow features develop in the reservoirs.

Fig. 1. 2D sketch illustrating the experimental flume equipped with (a) a free surface inlet channel, (b) a circular inlet jet (pressurized flow), and (c) 3D sketch depicting the experimental flume with a circular jet at the inlet.

In line with Peltier et al. (2014), the flow in shallow rectangular reservoirs is governed by nine parameters, namely the reservoir length, L_1, the reservoir width, B, the inlet channel width or jet diameter, b, the flow depth, H, the depth-averaged velocity in the inlet channel, U_{in}, the roughness height, k_s, the kinematic viscosity, ν, the gravitational acceleration, g, and the elevation of the centroid of the inlet section, Z_{jet}. The origin of the z axis is located at the bottom of the reservoir. The inlet velocity is calculated as $U_{in} = Q/(bH)$, with Q the inlet flow rate.

These nine dimensional parameters define the configurations of interest here: H, B, L_1, b, Z_{jet}, g, ν, U_{in}, and k_s. According to Vaschy Buckingham theorem, seven dimensionless parameters can be derived from the dimensional ones: the ratio of the reservoir width to the inlet width, B/b, reservoir length-to-width ratio, L_1/B, ratio of the flow depth to the reservoir width (i.e., shallowness parameter), H/B, Froude number, $\mathrm{Fr} = U_{in}/(gH)^{1/2}$, Reynolds number, $\mathrm{Re} = 4U_{in}H/\nu$, relative elevation of the inlet section centroid, Z_{jet}/H, and relative roughness height, k_s/H. In line with Peltier et al. (2014), k_s/H and Re can be merged into the friction number $S = \lambda B/H$, in which the friction coefficient, λ, is evaluated with Colebrook–White formula (Colebrook & White, 1937). The friction number, S, is defined here slightly differently from Chu et al. (2004) and Peltier et al. (2014). Indeed, since in the current tests the expansion width, ΔB, may differ between the reservoir inlet and outlet, the friction number, S, is defined here using the reservoir width, B, as a characteristic length. The geometric parameters L/B, and B/b, may be merged into the reservoir shape factor, SF (Dufresne et al., 2010; Peltier et al., 2014). In the experiments done here, the reservoir shape factor SF (short vs. long reservoirs), the Froude number (hence also S), the relative vertical positioning of the inlet jet (Z_{jet}/H) were systematically varied, while the flow shallowness, H/B was kept constant.

Table 1 lists the experimental conditions, with the corresponding non-dimensional numbers. For each inlet boundary condition, a short (L_1 = 1.05 m, SF = 4.65) and a long (L_1 = 2.00 m, SF = 8.87) reservoir were studied, considering three steady flow rates, Q, with a circular inlet jet (0.5, 1.75, 3.0 L/s) and two values (1.0 and 3.0 L/s) with a free surface inlet channel. Three inlet jet positions were tested: Z_{jet}/H = 0.20, 0.50, and 0.75. The Froude number ranges from 0.13 to 0.76, and the friction number, S, is in the range from 0.143 to 0.206.

Table 1. Program of experimental tests and type of observed flow pattern. S0 stands for symmetric jet without reattachment, O for meandering (oscillating) jet, U for unstable jet, and A1 or A1* for reattached jet in the reservoir.

Inlet	Test ID	L_1 (m)	ΔB (m)	SF	Q (10^{-4} m^3/s)	U_{in} (m/s)	Re (10^4)	Fr	S	Z_{jet}/H	Flow type
Rectangular channel	1	1.05	0.47	4.65	10.00	0.13	17.50	0.13	0.21	0.50	S0
	2				35.00	0.44	30.00	0.44	0.16		O
	3	2.00	0.45	8.87	10.00	0.13	17.50	0.13	0.21	0.50	A1
	4				35.00	0.44	30.00	0.44	0.16		A1
Jet	5	2.00	0.45	8.87	5.00	0.13	5.00	0.13	0.21	0.20	U
	6				17.50	0.44	17.50	0.44	0.16		U
	7				30.00	0.75	30.00	0.76	0.14		U
	8	1.05	0.47	4.65	5.00	0.13	5.00	0.13	0.21	0.20	U
	9				17.50	0.44	17.50	0.44	0.16		U
	10				30.00	0.75	30.00	0.76	0.14		U
	11	2.00	0.45	8.87	5.00	0.13	5.00	0.13	0.21	0.50	U
	12				17.50	0.44	17.50	0.44	0.16		A1
	13				30.00	0.75	30.00	0.76	0.14		A1
	14	1.05	0.47	4.65	5.00	0.13	5.00	0.13	0.21	0.50	A1*
	15				17.50	0.44	17.50	0.44	0.16		A1*
	16				30.00	0.75	30.00	0.76	0.14		A1*
	17	2.00	0.45	8.87	5.00	0.13	5.00	0.13	0.21	0.75	U
	18				17.50	0.44	17.50	0.44	0.16		A1*
	19				30.00	0.75	30.00	0.76	0.14		A1*
	20	1.05	0.47	4.65	5.00	0.13	5.00	0.13	0.21	0.75	A1*
	21				17.50	0.44	17.50	0.44	0.16		A1*
	22				30.00	0.75	30.00	0.76	0.14		A1*

The inflow discharge was measured with an electromagnetic flowmeter, which has an accuracy of 0.04%. The water level was controlled by a gate downstream of the flume. Its position was adapted for each flow rate to ensure a water depth, $H = 0.10$ m, in the reservoir. The water depth was measured using an ultrasonic probe (measurement accuracy of 1 mm) located 0.4 m upstream of the downstream

outlet. The Large-Scale Particle Image Velocimetry (LSPIV) technique was used for measuring surface velocity. As shown by Kantoush et al. (2008b) and Peltier et al. (2014), this technique provides accurate results in shallow reservoirs. The underlying principle consists in measuring the motion, between successive images, of visible tracers lying on the free surface. A Panasonic Lumix GH4 camera recording 1,920×1,080 pixels at a rate of 25 Hz was used. Videos were treated with the open-source software Fudaa-LSPIV. Images were orthorectified, and displacements of tracers between the images were calculated through statistical correlations. The floating tracer used was coarse sawdust 2 mm in diameter.

For a qualitative appraisal of 3D flow features in configurations with a circular jet at the inlet, a rod with attached pieces of wool was positioned at different locations in the reservoir. Additionally, 3D velocity profiles were measured with an acoustic Doppler velocity profiler (ADVP) probe (Nortek Vectrino). The probe has a 4-transducer orthogonal plane bistatic geometry. The measurements were taken over a distance of 3 cm staring 4 cm below the transducer head. For each probe location, 8,000 instantaneous velocity values over a period of 80 s were evaluated with a sampling rate of 100 Hz. To improve the quality of the signal, Glass Microspheres Spherical 110P8 particles were seeded in the flow. The despiking algorithm of Goring and Nikora (2002) was applied for removing spikes from velocity time series. The LSPIV and ADVP measurements showed a good repeatability of the measurements.

3. Results and discussion

A classification of the flow patterns observed in the twenty-two tested configurations is presented here. The main findings are briefly summarized in Section 3.1, mostly through Fig. 2. For the sake of comparison, Section 3.2 presents the flow fields observed for reservoirs equipped with a free surface inlet channel. Next, flow fields encountered in reservoirs with a circular inlet jet are characterized. The results distinguish between relatively short (Section 3.3) and long (Section 3.4) reservoirs.

3.1. General overview

For reservoirs with a free surface inlet channel, three types of flow patterns were observed: steady symmetric (detached) jet (S0), steady reattached jet (A1), or meandering jet (i.e., periodically

oscillating, O). In the case of a circular inlet jet, only two flow types were observed: either a steady reattached jet, or unstable flow field (i.e., varying over time in a chaotic manner). For long reservoirs, a flow pattern (A1) with a single reattachment point located in the upstream part of the reservoir is observed, like in the case of reservoirs with an open-channel inlet. For short reservoirs, a flow pattern (A1*) with a single reattachment point located in the downstream part of the reservoir is identified.

Fig. 2 provides an overview of the observations. Symbols are filled when a steady reattached jet was observed, and they are empty for unstable and meandering cases. The type of observed flow field depends on the type of inlet boundary condition (jet or channel), the reservoir geometry (length and positioning of the inlet jet), and the hydraulic boundary conditions (Fr and S). Cases with a free surface inlet channel are represented by a star at $Z_{jet}/H = 0.50$, while those with an inlet jet are represented by a square. The left and right parts of the symbols correspond to short and long reservoirs, respectively.

Fig. 2. Classification of observed flow patterns in short and long reservoirs: unstable (U), reattachment point located in the upstream part of the reservoir (A1), reattachment point located in the downstream part of the reservoir (A1*), symmetric without reattachment point (S0), and meandering (O). Notation Z_{jet}/H refers to the relative height of the centroid of the inlet pipe, and Fr is the Froude number.

3.2. Free surface inlet channel cases

For inlet free surface channel cases, the observed flow patterns are consistent with those reported in the literature, differing according to the reservoir geometry and hydraulic conditions (Fig. 2):

- In relatively short reservoirs (i.e., SF < 6.2), a steady symmetric flow pattern, corresponding to the flow type "S0" reported by Camnasio et al. (2011), Dufresne et al. (2010), and Kantoush (2008) was observed for the lower tested Froude number (Test 1). The corresponding surface velocity field obtained from LSPIV measurements is represented in non-dimensional form in Fig. 3(a), where the horizontal velocity $U = (u^2 + v^2)^{1/2}$ (u and v are the longitudinal and transversal components of velocity, respectively) is normalized by a reference velocity defined as $U_{ref} = Q/(b_0 H)$. The flow type is characterized by a straight jet from the inlet to the outlet, with large symmetric eddies on both reservoir sides and no jet reattachment. When the Froude

number is increased (Test 2), the flow jet oscillates (flow type O), in agreement with observations by Dufresne (2008), Kantoush (2008), and Peltier et al. (2014). In addition, the current results are in line with the findings of Peltier et al. (2014) stating that meandering jets form for a Fr > 0.20 and SF < 6.2.

- For the longer reservoir (SF > 6.2, Tests 3 and 4), a steady asymmetric flow pattern was found, characterized by a jet deflecting laterally and reattached to the left sidewall, as shown in Fig. 3b-c. This pattern (A1) was described by Camnasio et al. (2011), Dufresne et al. (2010), and Kantoush (2008). The flow asymmetry was attributed to the Coanda effect (Miozzi et al., 2010; Wille & Fernholz, 1965).

Fig. 3. Normalized surface velocity U/U_{ref} for short and long reservoirs with a free surface inlet channel: (a) Test 1, (b) Test 3, and (c) Test 4. U is the horizontal velocity defined as $U = (u^2 + v^2)^{1/2}$ (u and v are the longitudinal and transversal velocity components, respectively) and $U_{ref} = Q/(b_0 H)$ is a reference velocity. The white areas in the velocity maps correspond to regions where the velocity magnitude is particularly low.

3.3. Short reservoirs with a circular inlet jet

In relatively short reservoirs (SF < 6.2) with a circular jet at the inlet, two types of flow pattern were observed depending on the vertical positioning of the inlet jet: either a steady asymmetric pattern, or an unstable pattern (Fig. 2).

3.3.1. Steady asymmetric flow pattern

When the inlet jet was positioned either at mid-depth (i.e., $Z_{jet}/H = 0.5$, tests 14–16) or near the free surface (i.e., $Z_{jet}/H = 0.75$, tests 20–22), steady asymmetric flow patterns were observed regardless of the hydraulic boundary conditions (i.e., Froude and friction numbers). This flow type is labelled A1* in Fig. 2. As revealed by the surface velocity measurements (Fig. 4), this flow pattern involves one main recirculation, together with a secondary one and, in most cases, with smaller eddies in the upstream part of the reservoir. This flow pattern reattached jet with the reattachment point located in

the downstream part of the reservoir. The jet interacts with the free surface only at a certain distance downstream of the reservoir inlet. The magnitude of the normalized surface velocity is systematically greater for cases with an inlet jet closer to the surface than for the inlet jet at mid-depth.

For the lowest Froude number (tests 14 and 20), the normalized surface velocity magnitude reaches lower values than for the intermediate Froude number (tests 15 and 21). This may be attributed to a relatively higher jet momentum in the latter case, maintaining the jet more concentrated below the free surface. In contrast, the normalized surface velocity is relatively lower in tests 16 and 22 done under the highest Froude number. This hints at some competition between the increase in momentum and another process, which could be related to enhanced losses due to interactions between the jet and the quiescent water around it. In the case of the highest Froude number, the post-processing of the LSPIV measurements was also more challenging due to the presence of air bubbles at the surface and a higher difficulty to ensure a continuous injection of sawdust in a high-velocity flow.

Fig. 4. Normalized surface velocity U/U_{ref} for short reservoirs with a circular inlet jet. Fr is the Froude number, U is the horizontal velocity defined as $U = (u^2 + v^2)^{1/2}$ (u and v are the longitudinal and transversal velocity components, respectively) and $U_{ref} = Q/(b_0 H)$ is a reference velocity. The white areas in the velocity maps correspond to regions where the velocity magnitude is particularly low.

Unlike in the case of a free surface inlet channel, reservoirs with an inlet pressurized jet led to highly 3D flow features. This was qualitatively appreciated by placing a rod with wool filaments at different locations. Four filaments were used, uniformly distributed over the flow depth (i.e., positioned at 2, 4, 6, and 8 cm above the reservoir bottom). Similar results are found for configurations of a short reservoir with a circular inlet jet; Fig. 5 illustrates the case of Test 15. At the reservoir entrance, the filaments located at elevations 0.02 m and 0.04 m follow the direction of the main jet, while the two higher up filaments suggest that the flow velocity is almost zero close to the surface at this location (Fig. 5(a)). In the middle of the recirculation, flow velocity is close to zero and the four filaments wrap around the jet (Fig. 5(b)). Moving the rod toward the downstream end of the reservoir, all four filaments exhibit

a similar alignment, which indicates a velocity more uniformly distributed over the flow depth as encountered in the case of a free surface inlet channel (Fig. 5(c)).

Fig. 5. Images of filaments taken during Test 15 (short reservoir with inlet jet at $Z_{jet}/H = 0.50$), (a) at the reservoir entrance, (b) in the cent of the largest eddy, and (c) along the reservoir centerline close to its downstream end. The white areas in the velocity maps correspond to regions where the velocity magnitude is particularly low.

Measurements also were made with an ADVP probe. Fig. 6 shows transverse profiles of the longitudinal velocity for tests 14, 15, 20 and 21 along two cross-sections (Fig. 5) situated at $x = 0.50$ m (i.e. $x/b = 12.5$, Profile 1) and 0.89 m (i.e., $x/b = 22.5$, Profile 2). These profiles are situated in the intermediate field, found in the range $6 < x/b < 30$ for free jets (Abdel-Rahman, 2010), which is the transition region between the near field region where the flow characteristics are strongly impacted by the characteristics of the outlet nozzle and the far field where an auto-similarity profile could be found. The profiles of the longitudinal velocity measured profiles show a similar shape irrespective of the elevation in the flow layer; but the velocity magnitude varies with the elevation. Similarly, the transverse velocity profiles exhibit a comparable behavior, their data can be provided from the authors upon request. This observation implies that the flow pattern remains unchanged along the vertical in the transition region. In tests 14 and 20 (i.e., lower Froude number), the ratio of the maximum longitudinal velocity value measured using the ADVP exceeds that measured at the surface using the LSPIV by up to 20% in Profile 1 and by 30% to 40% in Profile 2. Similarly, in tests 15 and 21 (i.e., higher Froude number), the surface velocity measured using the LSPIV appears to be lower than the measurements obtained using the ADVP. This dissimilarity could indicate lower surface velocities in contrast to the measurements taken at a shallower relative depth, or it could be related to issues with the seeding material.

Fig. 6. Transversal profiles of longitudinal velocity in short reservoirs (tests 14, 15, 20, and 21) along two cross sections (x = 0.50 and 0.89 m), and for three elevations (z = 0.016, 0.036, and 0.050 m) with ADVP velocities, as well as the surface velocity measured with the LSPIV.

Fig. 7 overlays transversal profiles of normalized longitudinal velocity (U/U_{ref}) in short reservoirs for different elevations of the inlet pipe, and different hydraulic conditions. At mid-depth (i.e., z = 0.050 m), no significant trend emerges from the comparison between the velocity profiles for the inlet jet positions Z_{jet}/H = 0.50 (tests 14 and 15) and Z_{jet}/H = 0.75 (tests 20 and 21). Conversely, for profiles situated closer to the bottom, the normalized velocity tends to be greater for the inlet position Z_{jet}/H = 0.50 than for the position Z_{jet}/H = 0.75 (predominantly at x = 0.50 m, less visible at x = 0.89 m). Close to the bottom (i.e., z = 0.016 m), a difference also is observed both at x = 0.50 m and x = 0.89 m, highlighting the influence of the jet position on the velocity field.

Fig. 7. Transversal profiles of normalized longitudinal velocity (u/U_{ref}) in short reservoirs (tests 14, 15, 20, and 21), along two lateral cross sections x = 0.50 m and x = 0.89 m, and for four elevations (z = 0.016, 0.036, 0.050, and 0.10 m) measured with ADVP, as well as the surface velocity measured with the LSPIV.

3.3.2. Unstable flow pattern

When the inlet jet was located close to the reservoir bottom (Z_{jet}/H = 0.20, tests 8 to 10), an unstable flow pattern was obtained irrespective of the hydraulic conditions. The flow in the reservoir switched in a chaotic manner between different flow types, mostly reattaching alternately to one side wall to the other. Unstable flow fields were reported by Dufresne (2008) for rectangular shallow reservoirs equipped with a circular inlet jet, as well as by Camnasio et al. (2011) and Peltier et al. (2014) for reservoirs equipped with a free surface inlet channel. Camnasio et al. (2011) found two configurations with instability for SF equal to 4.09 and 4.48, corresponding to the transition from the symmetrical flow-field region to the asymmetrical flow-field region defined by Dufresne et al. (2010). The unstable

regime was observed by Peltier et al. (2014) for 6.2 < SF < 8.1 and Fr > 0.21. Fig. 8 shows surface velocity fields measured using the LSPIV for Test 9 at different times. Each velocity field was averaged over a relatively short period (4 s) to capture the time-evolution of the flow. During the first two minutes, the flow heads toward the left wall and two main eddies stand out, with their sizes changing over time. After running the test for one hour, the jet heads toward the right side. The transitions from one state to the other does not occur periodically but the switches seemed chaotic. Other intermediate states also were observed.

Fig. 8. Normalized surface velocity (U/U_{ref}) measured using the LSPIV for Test 9. Each displayed velocity was averaged over a short period of 4 s. U is the horizontal velocity defined as $U = (u^2 + v^2)^{1/2}$ (u and v are the longitudinal and transversal velocity components, respectively) and $U_{ref} = Q/(b_0H)$ is a reference velocity.

3.4. Long reservoirs with a circular inlet jet

In long reservoirs (SF > 6.2), when the inlet jet was positioned close to the bottom ($Z_{jet}/H = 0.20$, tests 5–7), an unstable flow type (referred to as U) was observed for all the hydraulic conditions, like in the case of short reservoirs. When the inlet jet was positioned at mid-depth or close to the surface (i.e., $Z_{jet}/H = 0.50$ and 0.75), the flow also was unstable for the slowest flow case (i.e., tests 11 and 17, Fr = 0.13), which differs from observations in short reservoirs. Increasing the Froude number (i.e., tests 12, 13, 18, and 19, Fr = 0.44 and 0.76), an asymmetric flow pattern with one main recirculation and small eddies in the upper part of the reservoir was found (Fig. 9). The ratio of the main recirculation's size to that of the secondary recirculation is greater for flow pattern A1 than for A1*.

Fig. 9. Normalized surface velocity (U/U_{ref}) measured with the LSPIV for long reservoirs with a circular inlet jet. Fr is the Froude number, U is the horizontal velocity defined as $U = (u^2 + v^2)^{1/2}$ (u and v are the longitudinal and transversal velocity components, respectively) and $U_{ref} = Q/(b_0H)$ is a reference velocity.

Fig. 10 shows transverse profiles of the horizontal velocity along two cross sections, at x = 1.00 m (i.e., x/b = 25, intermediate field) and x = 1.70 m (i.e., x/b = 42.5, far field). Observations in these profiles shows the attachment of the jet to the left sidewall as well as the presence of a recirculation, corresponding to flow pattern A1.

- For an inlet jet positioned at mid-depth (tests 12 and 13), the ADVP velocity profiles at three vertical positions and the LSPIV profile remain similar in shape but differ in magnitude. In Test 12, the maximum positive longitudinal velocity measured with ADVP at z = 0.016 m (i.e., close to the bottom) exceeds the surface velocity by a factor of 2.4 at x = 1.00 m, whereas ADVP and LSPIV measurements are mostly similar at x = 1.70 m except for the reverse flow ($u < 0$) of the profile measured using the ADVP close to the bottom, which still exhibits higher velocity magnitude compared to the LSPIV. Compared to the cross-section at x = 1.00 m, the maximum velocity measured using the LSPIV and ADVP are more uniform at x = 1.70 m, i.e., at a greater distance from the reservoir entrance.
- Increasing the Froude number (Test 13), the maximum positive velocity measured with the ADVP at x = 1.00 m was found to be 1.4 times higher than the corresponding value measured with the LSPIV. At x = 1.70 m, this difference is again strongly reduced, like in the case of Test 12. LSPIV and ADVP measurements exhibit less consistency, which may be attributed to the difficulty of ensuring a homogeneous presence of sawdust. On the other hand, it is observed that the magnitude of velocities measured using the ADVP decreases as one approaches the bottom (z = 0.016 m).
- For a jet located close to the free surface and a comparatively low Froude number (Test 18), the profiles measured at x = 1.00 m using the ADVP and the LSPIV are all very close to each other, both in terms of shape and magnitude. The maximum velocity recorded using the ADVP and the LSPIV differ by no more than 6%. At x = 1.70 m, the maximum velocity measured using the LSPIV exceeds the value obtained using the ADVP by about 25%, revealing greater surface velocities compared to the measurements recorded at a lower relative depths. It is

consistently observed that the magnitude of velocities measured using the ADVP decreases as one gets closer to the bottom (z = 0.016 m).

- When the Froude number is higher (Test 19), the maximum velocities measured by the ADVP exceed those obtained by the LSPIV by almost 40% at x = 1.00 m. Furthermore, similar to Test 13, the LSPIV measurements exhibit reduced accuracy at this cross section, the LSPIV measurements exhibit more scatter attributed to the sawdust injection. A general observation that remains available regarding the measurements of profile 2: The velocity intensity rises as one moves from the bottom towards the middle of the water column.

The results indicate that a jet within a confined environment loses its self-similarity (Pope, 2000). Theoretical models have been proposed to describe self-sustained oscillations of a confined jet (e.g., Righolt et al., 2015).

Fig. 10. Transversal profiles of longitudinal velocity in long reservoirs (tests 12, 13, 18, and 19), along two lateral cross sections x = 1.00 m and x = 1.70 m, and for three elevations (z = 0.016, 0.036, and 0.050 m) measured using the ADVP, as well as the surface velocity measured using the LSPIV.

Fig. 11 compares transversal profiles of longitudinal velocity normalized by the reference velocity for tests 12, 13, 18, and 19. In most cases, no significant trend can be detected by comparing the profiles of normalized velocity (e.g., at z = 0.036 m and at z = 0.050 m), irrespective of the considered cross section (i.e., both at x = 1.00 m and x = 1.70 m). This suggests that, at theses distances from the inlet, the flow fields are not substantially altered when the position of the inlet jet is varied. In contrast, near the bottom (at z = 0.0016 m), longitudinal velocities are found to be higher for Test 12, in which the inlet jet is positioned at Z_{jet}/H = 0.50. Similarly, at the surface, longitudinal velocities are higher in Test 18 compared to the others, as Test 18 corresponds to Z_{jet}/H = 0.75.

Fig. 11. Transversal profiles of normalized longitudinal velocity (u/U_{ref}) in long reservoirs (tests 12, 13, 18, and 19), along two lateral cross sections x = 1.00 m and x = 1.70 m, and for four elevations (z = 0.016, 0.036, 0.050, and 0.10 m) measured using the ADVP, as well as the surface velocity measured with the LSPIV.

4. Conclusions

Flow patterns in rectangular shallow reservoirs were analyzed using laboratory experiments, with particular focus on the effect of inlet boundary conditions: free surface rectangular channel vs circular inlet jet. In both cases, the reservoir outlet was a free surface channel. Twenty-two experimental tests were done, in which the reservoir length, the hydraulic boundary conditions, and the vertical position of the inlet jet (near bottom, mid-depth or near surface) were varied. For a free surface inlet channel, the observed flow fields agreed with previous studies in similar configurations involving either steady or meandering jets in the reservoir. For a circular inlet jet, the current experimental results revealed that the type of flow pattern is influenced by the vertical positioning of the inlet jet, by the reservoir geometry (short vs long) and, in some cases, by the hydraulic boundary conditions (Froude and friction numbers). When the inlet circular jet is positioned near the reservoir bottom, an unstable flow type (i.e., switching over time in a chaotic manner) was observed irrespective of the reservoir length and of the hydraulic boundary conditions. The same type of unstable flow pattern was observed for a relatively long reservoir under the lowest Froude number condition, regardless of the vertical positioning of the inlet jet. In all other tested configurations, a steady reattached jet was found, distinguishing an asymmetrical flow with the reattachment point in the downstream part of the reservoir for short reservoir, and an asymmetrical flow with the reattachment point in the upstream part of the reservoir for long reservoirs.

Compared to a free surface inlet channel, an inlet jet boundary condition induces a more three-dimensional flow in the near field of the inlet. The analysis and comparison of the ADVP profiles at different vertical positions and LSPIV profiles at the surface indicate that the longitudinal velocity

distribution along the vertical axis undergoes variations due the jet's position, the Froude number, and its longitudinal location within the reservoir.

The current experimental study is an addition to existing research on the complex hydrodynamics of shallow reservoirs. Nonetheless, real-world shallow reservoirs show more complex configurations, which appear worth of being tested in future laboratory studies. These should consider varying the positioning of the inlet pipe over the reservoir width, as well as testing various relative sizes of the inlet pipe compared to the reservoir width and the flow depth. In real structures, the inlet pipe is not necessarily normal to the reservoir side, and it can even be positioned along a reservoir side which is not opposite to the side where the reservoir outlet is located. The influence of such geometric variations can be partly explored based on validated computational models. Collecting experimental observations on a larger setup remains important to enable exploring more shallow configurations while also clarifying the influence of scale effects. More laboratory tests are ongoing, paving the way for further analyses on sediment transport and sediment deposition in such reservoirs, as well as on the feedback of morphodynamic evolution on the flow pattern. The new experimental data presented here are valuable for assessing the performance of 2D and 3D computational models.

Notation

B = Reservoir width (m)

b = Inlet channel width or diameter of the inlet jet (m)

b_o = Outlet channel width (m)

D = Hydraulic diameter of the pipe or channel (m)

Fr = Froude number

g = Gravitational acceleration (m/s^2)

H = Water depth (m)

k_s = Roughness height (m)

L_1 = Reservoir length (m)

L_e = Recommended entrance length (m)

Q = Inlet flow rate (m^3/s)

Re = Reynolds number

S = Non-dimensional reservoir friction number

SF = Non-dimensional reservoir shape parameter

u = Horizontal velocity component in x direction (m/s)

U = Horizontal velocity (m/s)

U_{in} = Theoretical velocity at the inlet channel (m/s)

U_{ref} = Theoretical mean plug flow velocity in the reservoir (m/s)

v = Horizontal velocity component in y direction (m/s)

w = Vertical velocity component (m/s)

x = Streamwise coordinate (m)

y = Transverse coordinate (m)

z = Vertical coordinate (m)

Z_{jet} = Elevation of the inlet pipe centroid above the reservoir bottom (m)

ΔB = Width of the sudden expansion (m)

λ = Friction coefficient

ν = Water kinematic viscosity (m^2/s)

Acknowledgements

This research is partially funded by Association Nationale de Recherche et de la Technologie (ANRT) Grant No. [CIFRE #2019/1262].

References

Abbott, D. E. & Kline, S.J. (1962) Experimental investigation of subsonic turbulent flow over single and double backward facing steps. *Journal of Basic Engineering*, *84*(3), 317–325.

Abdel-Rahman, A. (2010). A review of effects of initial and boundary conditions on turbulent jets. *WSEAS Transactions on Fluid Mechanics*, *5*, 257–275.

Adamsson, A., Bergdahl, L., & Lyngfelt, S. (2005). Measurement and three-dimensional simulation of flow in a rectangular detention tank. *Urban Water Journal*, *2*(4), 277–287.

Casarsa, L., & Giannattasio, P. (2008). Three-dimensional features of the turbulent flow through a planar sudden expansion. *Physics of Fluids*, *20*, 1–15.

Camnasio, E., Orsi, E., & Schleiss, A. (2011). Experimental study of velocity fields in rectangular shallow reservoirs. *Journal of Hydraulic Research*, *49*(3), 352–358.

Camnasio, E., Erpicum, S., Orsi, E., Pirotton, M., Schleiss, A. J., & Dewals, B. (2013). Coupling between flow and sediment deposition in rectangular shallow reservoirs. *Journal of Hydraulic Research*, *51*(5), 535–547.

Çengel, Y. A., & Cimbala, J. M. (2018). *Fluid Mechanics: Fundamentals and Applications* (4th edn). New York: McGraw-Hill.

Choufi, L., Kettab, A., & Schleiss, A. J. (2014). Effet de la rugosité du fond d'un réservoir rectangulaire à faible profondeur sur le champ d'écoulement. *La Houille Blanche*, (5), 83–92. (*in French*)

Chu, V. H., Liu, F., & Altai, W. (2004). Friction and confinement effects on a shallow recirculating flow. *Journal of Environmental Engineering and Science*, *3*, 463–475.

Colebrook, C. F., & White, H. L. (1937). Experiments on the transmission of heat and pressure in pipes. *Journal of the Institution of Civil Engineers*, *5*(4), 133–156.

Dewals, B., Kantoush, S., Erpicum, S., Pirotton, M., & Schleiss, A. J. (2008). Experimental and numerical analysis of flow instabilities in rectangular shallow basins. *Environmental Fluid Mechanics*, *8*, 31–54.

Dufresne, M. (2008). *La modélisation 3D du transport solide dans les bassins en assainissement : du pilote expérimental à l'ouvrage réel. [Three-dimensional modelling of sediment transport in sewer detention tanks: physical model and real-life application]*. Département de Génie Civil. Ph.D. dissertation, Université de Strasbourg. (*in French*)

Dufresne, M., Dewals, B. J., Erpicum, S., Archambeau, P., & Pirotton, M. (2010). Classification of flow patterns in rectangular shallow reservoirs. *Journal of Hydraulic Research*, *48*(2), 197–204.

Durst, F., Pereira, J. C. F., & Tropea, C. (1993). The plane symmetric sudden-expansion flow at low Reynolds numbers. *Journal of Fluid Mechanics*, *248*, 567–581.

Escudier, M. P., Oliveira, P. J., & Poole, R. J. (2002). Turbulent flow through a plane sudden expansion of modest aspect ratio. *Physics of Fluids*, *14*, 3641–3654.

Goring, D., & Nikora, V. (2002). Despiking acoustic doppler velocimeter data. *Journal of Hydraulic Engineering*, *128*, 117–126.

Kantoush, S. A. (2008). *Experimental study on the influence of the geometry of shallow reservoirs on flow patterns and sedimentation by suspended sediments*. La Faculté de l'Environnement, Architectural et Construit. Ph.D. dissertation. Ecole Polytechnique Fédérale de Lausanne.

Kantoush, S. A., Bollaert, E., & Schleiss, A. J. (2008a). Experimental and numerical modelling of sedimentation in a rectangular shallow basin. *International Journal of Sediment Research*, *23*, 212–232.

Kantoush, S. A., De Cesare, G., Boillat, J. L. & Schleiss, A. J. (2008b). Flow field investigation in a rectangular shallow reservoir using UVP, LSPIV and numerical modelling. *Flow Measurement and Instrumentation, 19*(3–4), 139–144.

Mehta, P. F. (1981). Separated flow through large sudden expansions. *Journal of the Hydraulics Division*, *107*(HY4), 451.

Miozzi, M., Lalli, F., & Romano, G. P. (2010) Experimental investigation of a free-surface turbulent jet with Coanda effect. *Experiments in Fluids*, *49*, 341–353.

Miozzi, M., & Romano, G. P. (2020). Propagation of perturbations and meandering in a free surface shallow water jet. *Experiments in Fluids*, *61*, 192.

Miranda, D. A., Reis, A. M., Alves, E., Cardoso, A. H., & Coelho, M. M. L. P. (2018). Experimental study of the influence of inlet and outlet conditions on the flow pattern of a rectangular shallow reservoir. Dans Daniel Bung, Blake Tullis. In: Proceedings of the 7th IAHR International Symposium on Hydraulic Structures, May 15–18, 2018, Aachen, Germany.

Moallemi, N., & Brinkerhoff, J. R. (2016). Numerical analysis of laminar and transitional flow in a planar sudden expansion. *Computers & Fluids*, *140*, 209–221.

Peltier, Y., Erpicum, S., Archambeau, P., Pirotton, M., & Dewals, B. (2014). Experimental investigation of meandering jets in shallow reservoirs. *Environmental Fluid Mechanics*, *14*(3), 699–710.

Pope, S. (2000). *Turbulent Flows*. Cambridge, UK: Cambridge University Press.

Righolt, B. W., Kenjeres, S., Kalter, R., Tummers, M. J., & Kleijn, C. R. (2015). Dynamics of an oscillating turbulent jet in a confined cavity. *Physics of Fluids*, *27*(9), 095107.

Restivo, A., & Whitelaw, J. H. (1978). Turbulence characteristics of the flow downstream of a symmetric, plane sudden expansion. *Journal Fluids Engineering*, *100*, 308.

Shoarinezhad, W., Wieprecht, S., Kantoush, S. A., & Haun, S. (2023). Applying optimization methods for automatic calibration of 3D morphodynamic numerical models of shallow reservoirs: comparison between lozenge- and hexagon-shaped reservoirs. J*ournal of Hydroinformatics*, *25*(1), 85–100.

Schleiss, A. J., Franca, M. J., Juez, C., & De Cesare, G. (2016). Reservoir sedimentation. *Journal of Hydraulic Research*, *54*, 595–614.

Wille, R., & Fernholz, H. (1965). Report on the first European mechanics colloquium, on the Coanda effect. *Journal of Fluid Mechanics*, *23*(4), 801–819.

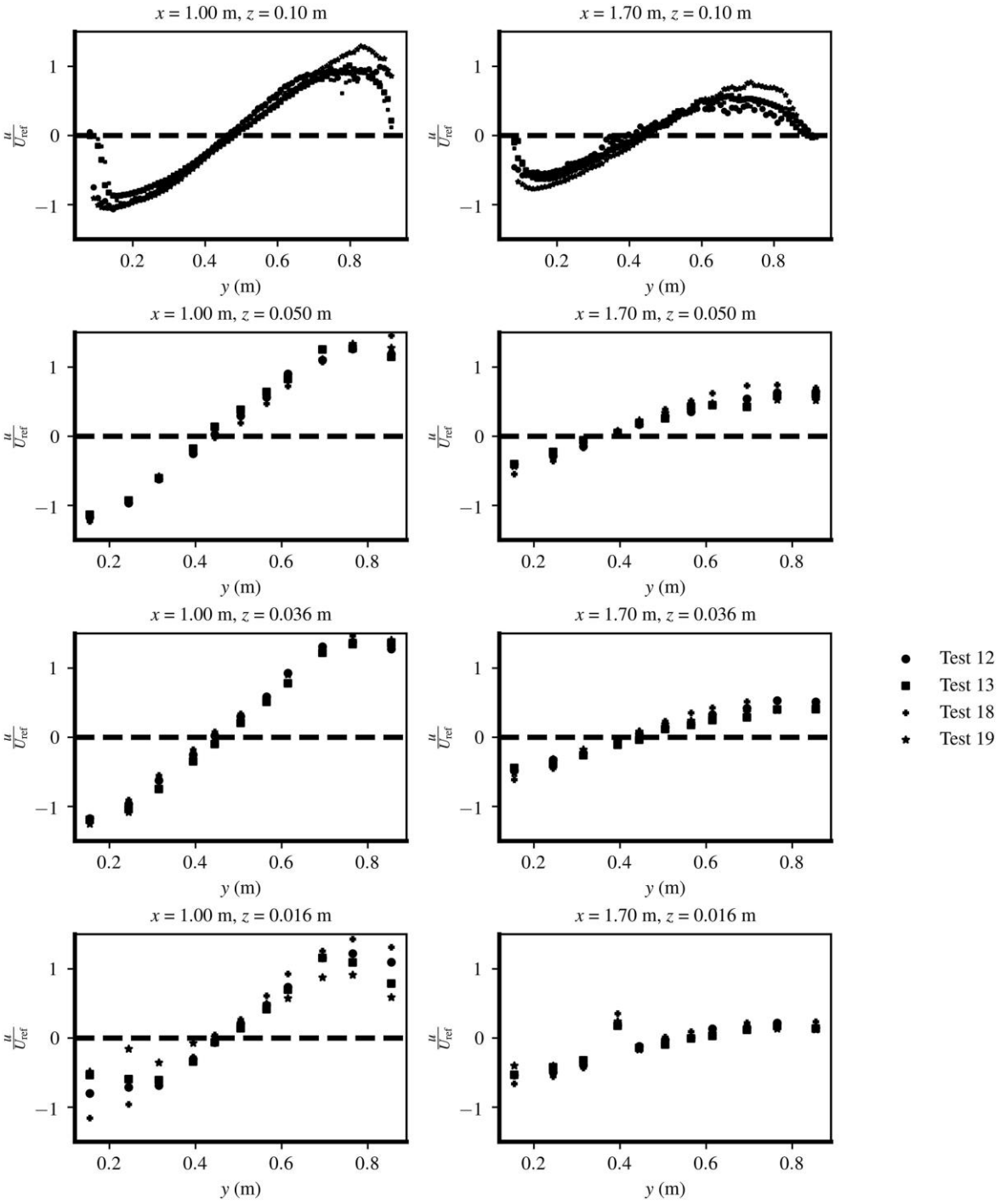
x = 1.00 m, z = 0.10 m
x = 1.70 m, z = 0.10 m
x = 1.00 m, z = 0.050 m
x = 1.70 m, z = 0.050 m
x = 1.00 m, z = 0.036 m
x = 1.70 m, z = 0.036 m
x = 1.00 m, z = 0.016 m
x = 1.70 m, z = 0.016 m
u/U_ref
y (m)
Test 12
Test 13
Test 18
Test 19

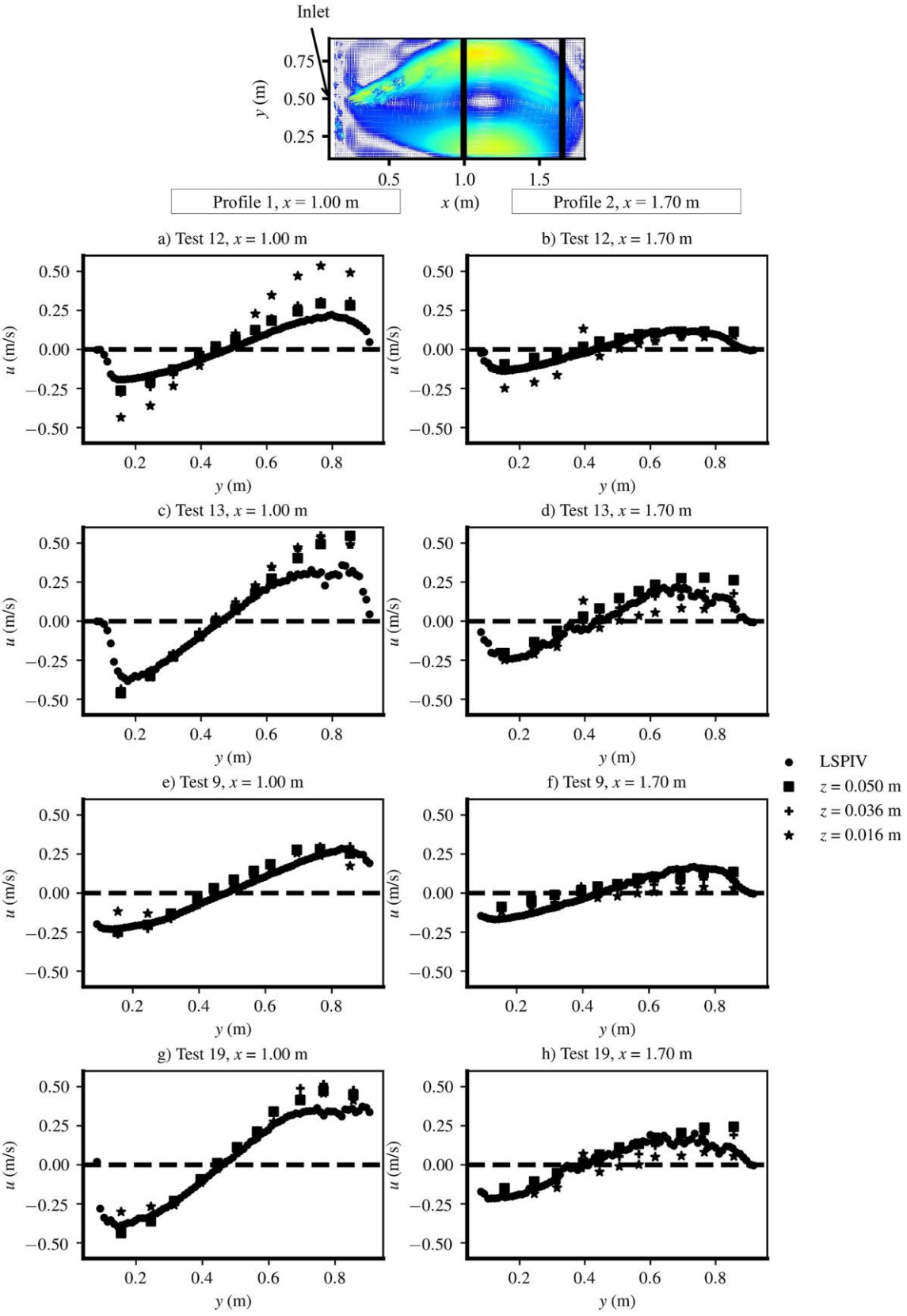
Inlet
0.75
0.50
0.25
y (m)
0.5
1.0
1.5
x (m)
Profile 1, x = 1.00 m
Profile 2, x = 1.70 m
a) Test 12, x = 1.00 m
b) Test 12, x = 1.70 m
c) Test 13, x = 1.00 m
d) Test 13, x = 1.70 m
e) Test 9, x = 1.00 m
f) Test 9, x = 1.70 m
g) Test 19, x = 1.00 m
h) Test 19, x = 1.70 m
u (m/s)
y (m)
0.50
0.25
0.00
−0.25
−0.50
0.2
0.4
0.6
0.8
LSPIV
z = 0.050 m
z = 0.036 m
z = 0.016 m

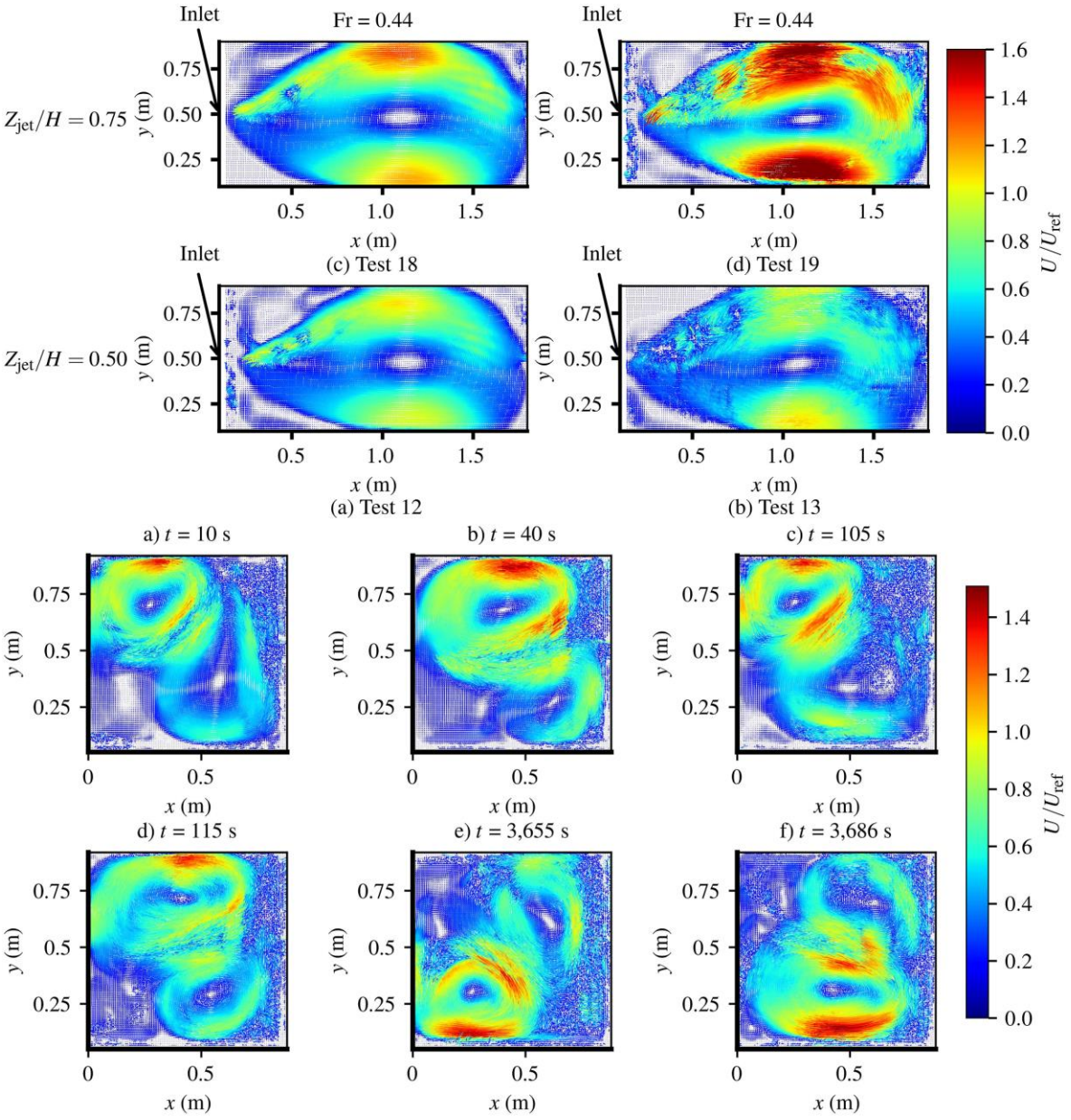
Inlet
Fr = 0.44
$Z_{jet}/H = 0.75$
$Z_{jet}/H = 0.50$
y (m)
x (m)
(a) Test 12
(b) Test 13
(c) Test 18
(d) Test 19
U/U_{ref}
a) t = 10 s
b) t = 40 s
c) t = 105 s
d) t = 115 s
e) t = 3,655 s
f) t = 3,686 s

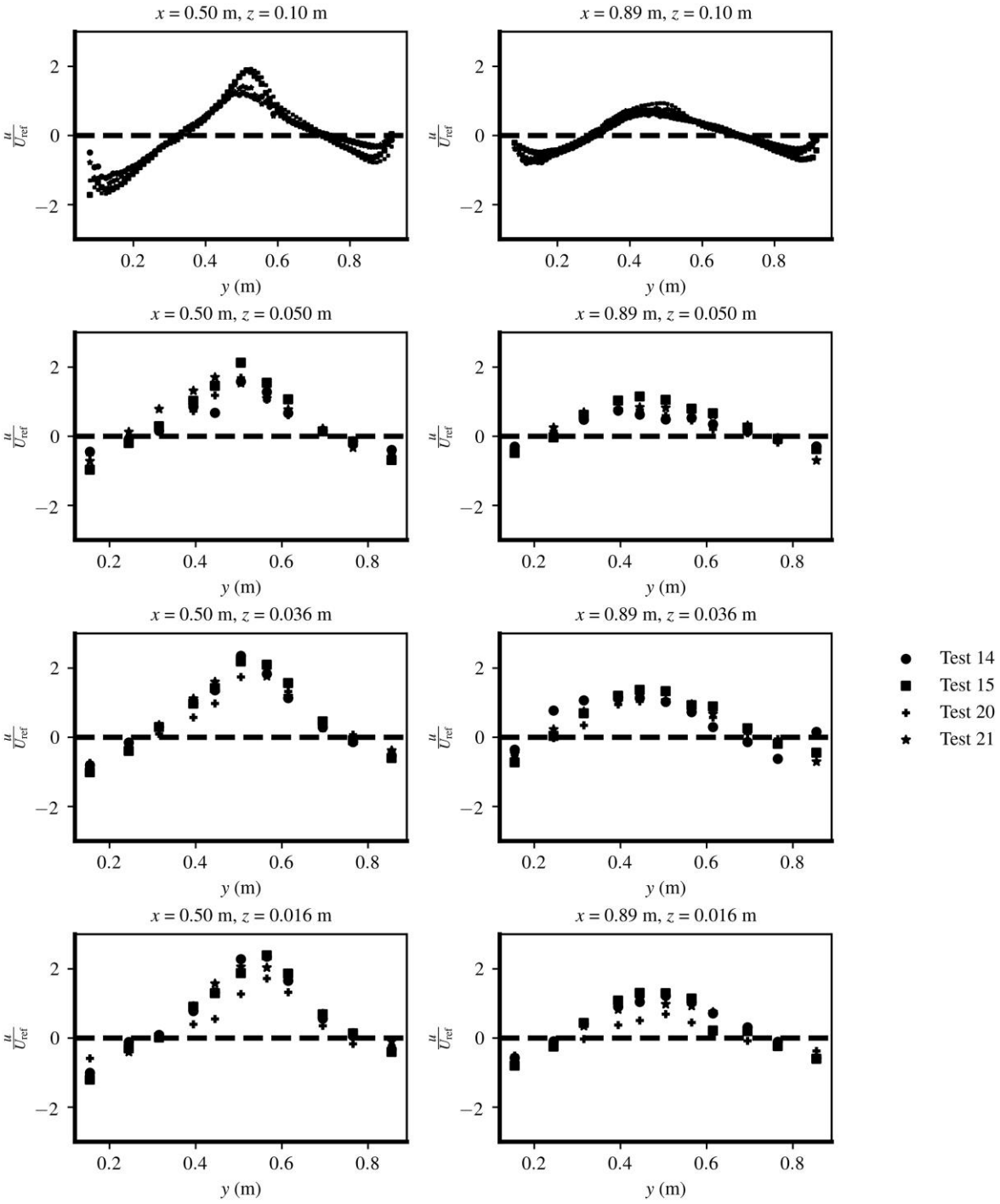
x = 0.50 m, z = 0.10 m
x = 0.89 m, z = 0.10 m
x = 0.50 m, z = 0.050 m
x = 0.89 m, z = 0.050 m
x = 0.50 m, z = 0.036 m
x = 0.89 m, z = 0.036 m
x = 0.50 m, z = 0.016 m
x = 0.89 m, z = 0.016 m
u/U_ref
y (m)
2
0
−2
0.2
0.4
0.6
0.8
Test 14
Test 15
Test 20
Test 21

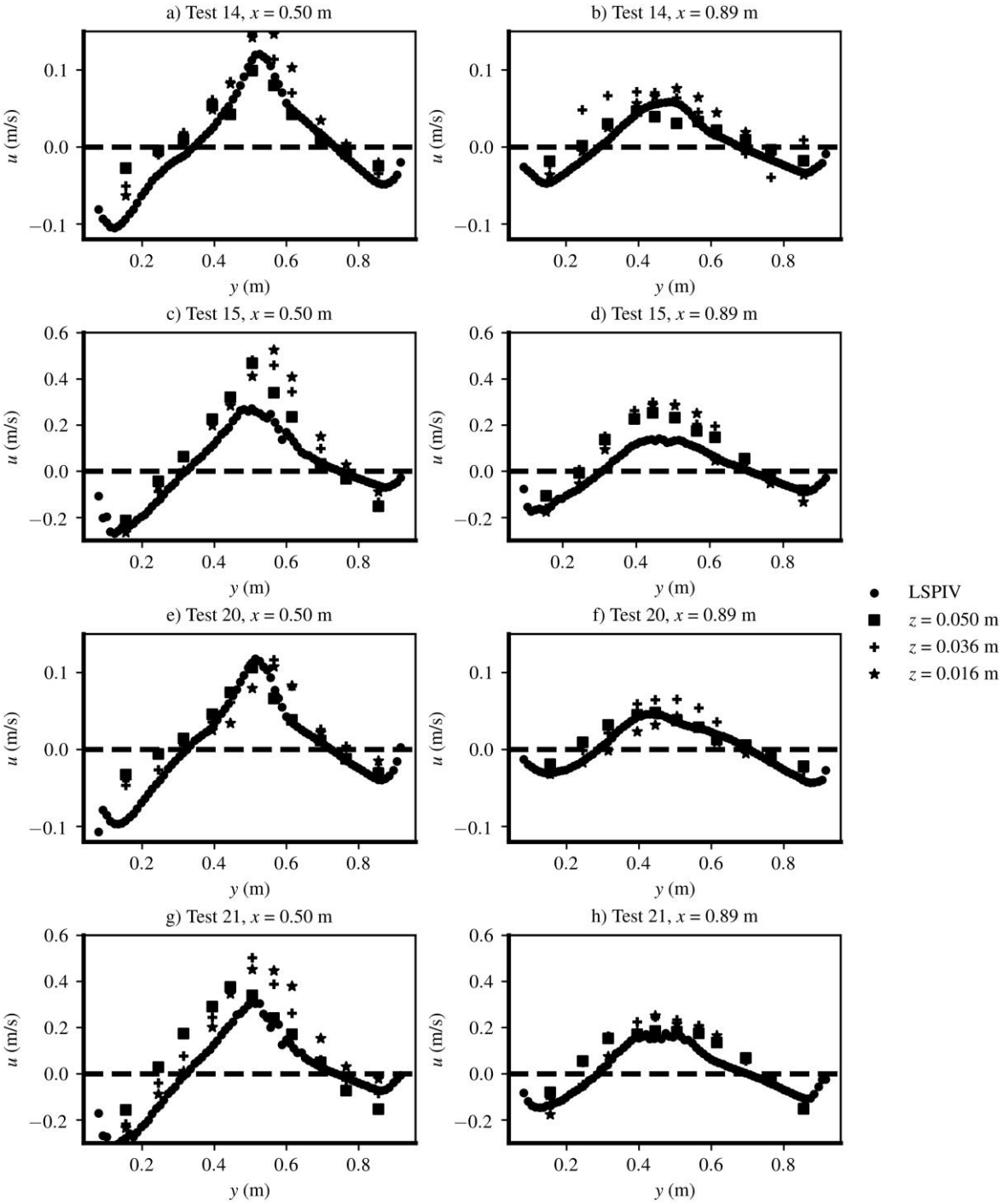
a) Test 14, x = 0.50 m
b) Test 14, x = 0.89 m
c) Test 15, x = 0.50 m
d) Test 15, x = 0.89 m
e) Test 20, x = 0.50 m
f) Test 20, x = 0.89 m
g) Test 21, x = 0.50 m
h) Test 21, x = 0.89 m
u (m/s)
y (m)
LSPIV
z = 0.050 m
z = 0.036 m
z = 0.016 m

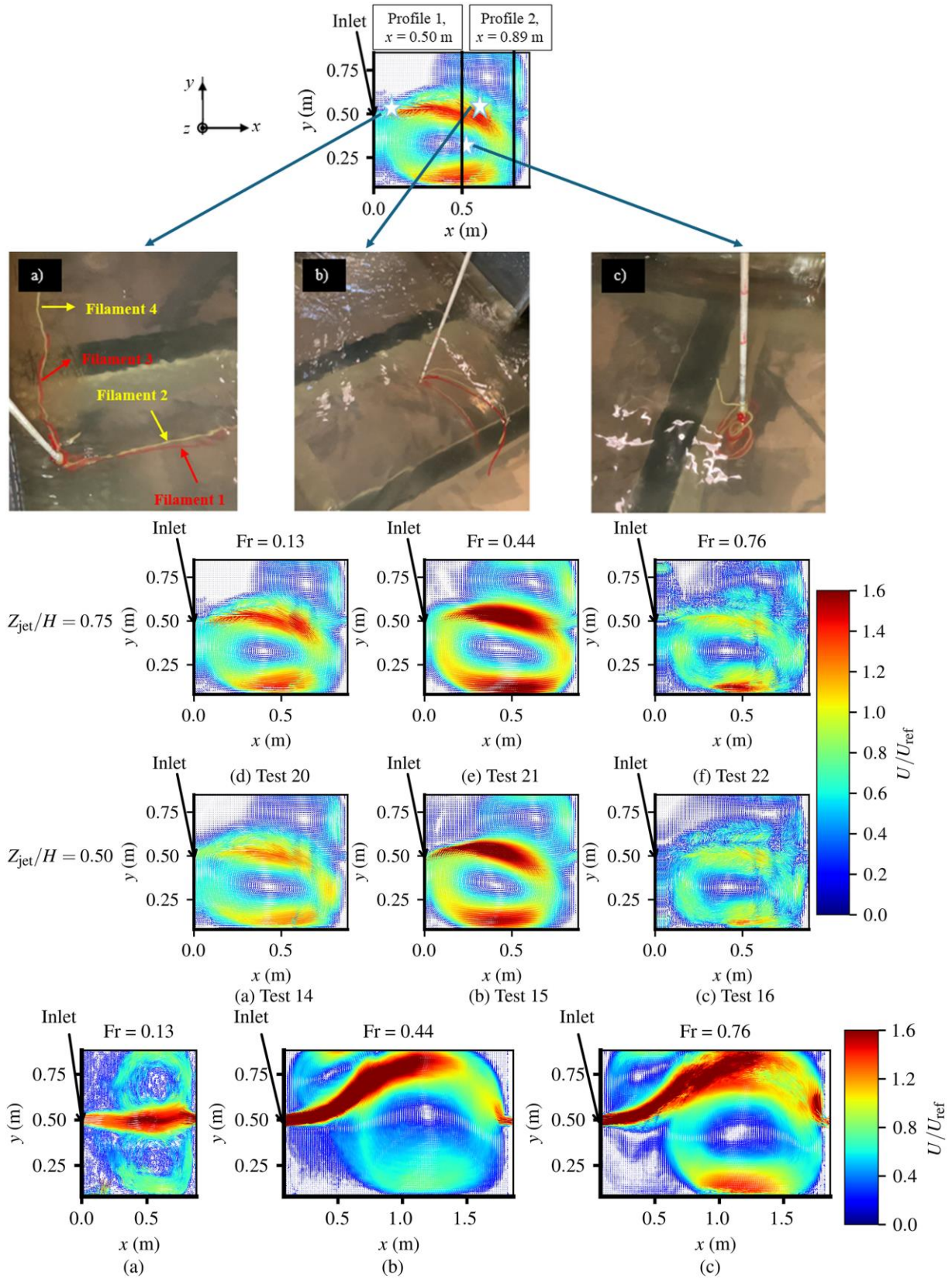
Inlet
Profile 1, x = 0.50 m
Profile 2, x = 0.89 m
y (m)
x (m)
a)
b)
c)
Filament 4
Filament 3
Filament 2
Filament 1
Fr = 0.13
Fr = 0.44
Fr = 0.76
$Z_{jet}/H = 0.75$
$Z_{jet}/H = 0.50$
(d) Test 20
(e) Test 21
(f) Test 22
(a) Test 14
(b) Test 15
(c) Test 16
U/U_{ref}

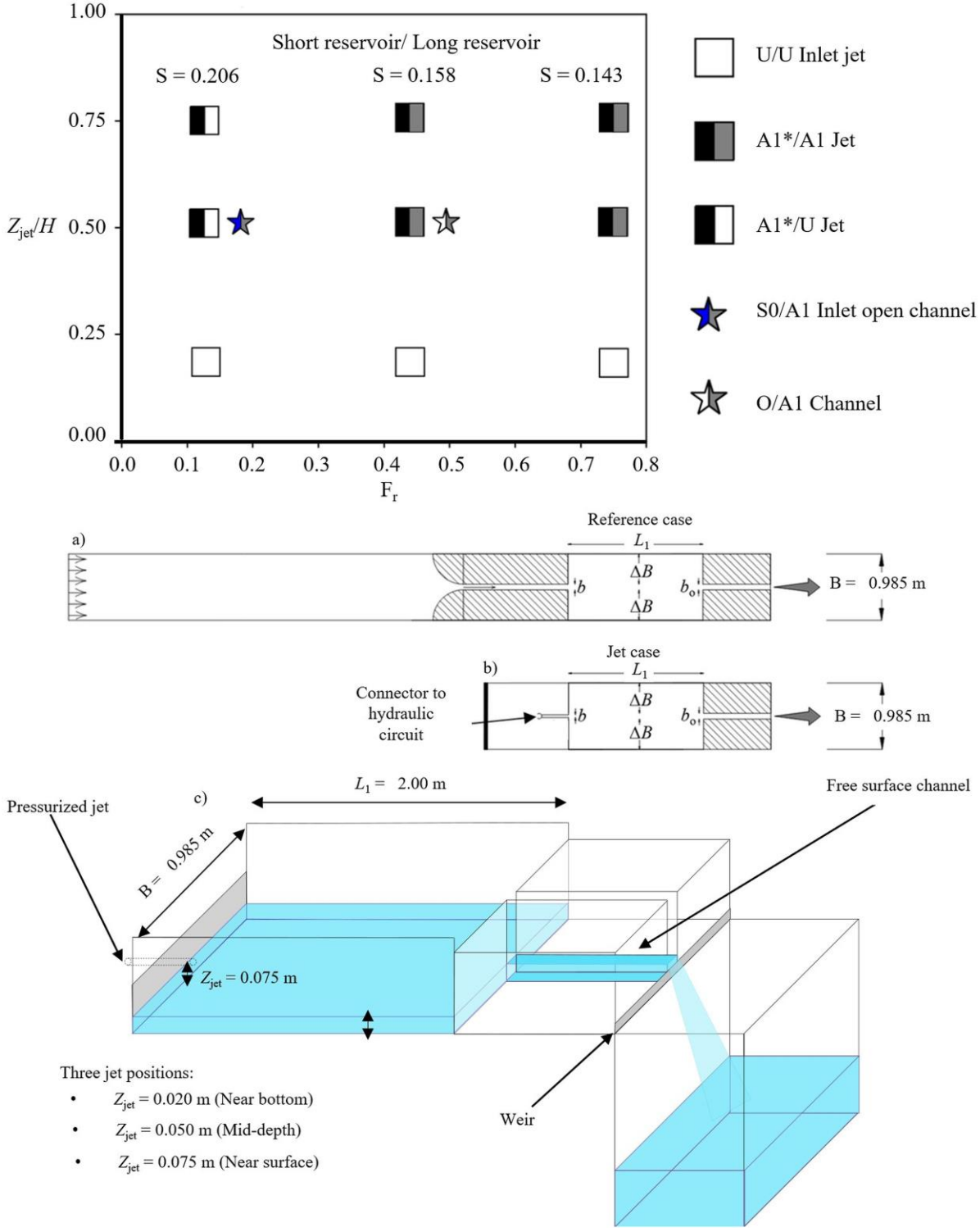
Short reservoir/ Long reservoir
S = 0.206
S = 0.158
S = 0.143
Z_{jet}/H
1.00
0.75
0.50
0.25
0.00
0.0
0.1
0.2
0.3
0.4
0.5
0.6
0.7
0.8
F_r
U/U Inlet jet
A1*/A1 Jet
A1*/U Jet
S0/A1 Inlet open channel
O/A1 Channel
a)
Reference case
L_1
ΔB
b
b_o
B = 0.985 m
b)
Jet case
Connector to hydraulic circuit
c)
L_1 = 2.00 m
Pressurized jet
B = 0.985 m
Z_{jet} = 0.075 m
Free surface channel
Weir
Three jet positions:
• Z_{jet} = 0.020 m (Near bottom)
• Z_{jet} = 0.050 m (Mid-depth)
• Z_{jet} = 0.075 m (Near surface)

Declaration of interests

☒ The authors declare that they have no known competing financial interests or personal relationships that could have appeared to influence the work reported in this paper.

☐The authors declare the following financial interests/personal relationships which may be considered as potential competing interests: